JOURNAL OF THE MECHANICAL BEHAVIOR OF BIOMEDICAL MATERIALS 61 (2016) 87–95

Available online at www.sciencedirect.com

ScienceDirect

www.elsevier.com/locate/jmbbm


Research paper

# Bioinspired polydimethylsiloxane-based composites with high shear resistance against wet tissue

*Sarah C.L. Fischer*[a,b,c,d], *Oren Levy*[c,d], *Elmar Kroner*[a], *René Hensel*[a], *Jeffrey M. Karp*[c,d,*], *Eduard Arzt*[a,b,**]

[a]*INM – Leibniz Institute for New Materials, Campus D2 2, 66123 Saarbrücken, Germany*
[b]*Department of Materials Science and Engineering, Saarland University, Campus D2 2, 66123 Saarbrücken, Germany*
[c]*Harvard-MIT Division of Health Science and Technology, Massachusetts Institute of Technology, Cambridge, MA 02139, USA*
[d]*Division of Biomedical Engineering, Department of Medicine, Brigham and Women's Hospital, Harvard Medical School, Boston, MA 02139, USA*

ARTICLE INFO

*Article history:*
Received 15 October 2015
Accepted 18 January 2016
Available online 25 January 2016

*Keywords:*
Polydimethylsiloxan (PDMS)
Composite
Shear resistance
Wound closure
Bioinspired

ABSTRACT

Patterned microstructures represent a potential approach for improving current wound closure strategies. Microstructures can be fabricated by multiple techniques including replica molding of soft polymer-based materials. However, polymeric microstructures often lack the required shear resistance with tissue needed for wound closure. In this work, scalable microstructures made from composites based on polydimethylsiloxane (PDMS) were explored to enhance the shear resistance with wet tissue. To achieve suitable mechanical properties, PDMS was reinforced by incorporation of polyethylene (PE) particles into the pre-polymer and by coating PE particle reinforced substrates with parylene. The reinforced microstructures showed a 6-fold enhancement, the coated structures even a 13-fold enhancement in Young's modulus over pure PDMS. Shear tests of mushroom-shaped microstructures (diameter 450 μm, length 1 mm) against chicken muscle tissue demonstrate first correlations that will be useful for future design of wound closure or stabilization implants.



## 1. Introduction

Since the development of versatile, customizable, and biodegradable biomaterials, the concepts of wound closure, essential for most tissue injuries ranging from small lacerations to major surgeries, have undergone a significant evolution (Chu et al., 1996; Menaker, 2001; Ratner and Bryant, 2004). Each wound exhibits different characteristics and, thus, the closure procedure is usually subject to the surgeon's expertise (Bennett, 1988; Scheidel and Hohl, 1987). As an example,

*Corresponding author at: Harvard-MIT Division of Health Science and Technology, Massachusetts Institute of Technology, Cambridge, MA 02139, USA.
**Corresponding author at: INM – Leibniz Institute for New Materials, Campus D2 2, 66123 Saarbrücken, Germany.
E-mail addresses: jeffkarp.bwh@gmail.com (J.M. Karp), eduard.arzt@leibniz-inm.de (E. Arzt).

http://dx.doi.org/10.1016/j.jmbbm.2016.01.014

hernia surgery provides an interesting and sophisticated wound closure concept. The disease consists in a protrusion of inner organs through a weak part of muscular layer towards the abdominal wall. Nowadays, polymer meshes, which cover the whole affected area, are utilized to reinforce the weak tissue and to keep the organs in place (Brown and Finch, 2010; Cobb et al., 2006). However, this treatment is not sufficient to enable a contraction of the weak tissue and requires additional fixtures such as stitches to prevent reoccurrence. Novel hernia meshes may be equipped with mechanically interlocking structures to enable self-fixation and contraction of the wound cover in contact with the weak tissue such as the ProGrip (Covidien, Dublin, Ireland) (Birk and Pardo, 2012; Pedano et al., 2012). Mostly in-vivo studies were performed with this type of mesh (Birk and Pardo, 2012; Chastan, 2009; Hollinsky et al., 2009; Jorgensen et al., 2013; Kolbe et al., 2010; Pedano et al., 2012; Sanders et al., 2013; Zhang et al., 2013) but no in-depth systematic investigation of the mechanical behavior exists.

Multiple examples for interlocking and adhesive microstructures can be found in nature, e.g. on plants (Koch et al., 2009) or on animals (Arzt et al., 2003; Gorb et al., 2001; Gorb, 1998). In contrast to penetrating systems (Cho et al., 2012; Yang et al., 2013), these structures allow the build-up of high shear forces solely with structure-based fixation (Bin Khaled and Sameoto, 2014; Glass et al., 2010). Additionally, many fixation mechanisms in nature are switchable, allowing multiple attachment and detachment cycles without large damage of the structures or substrate (Chary et al., 2013; Paretkar et al., 2013). These examples highlight the potential of translating nature-inspired microstructures into technical and medical applications (Gorb et al., 2007; Lee et al., 2015; Pang et al., 2012), but exact replication of biological structures is challenging.

Polydimethylsiloxane (PDMS) is a suitable material for the fabrication of microstructures and use in biomedical systems (Pang et al., 2015, 2013). Due to its elastic behavior the material is used to mimic animal adhesive systems such as the gecko's fibrillar structures (Del Campo et al., 2007; Zhou et al., 2013). The influence of the geometry and hierarchy of microstructures were explored experimentally and theoretically (Aksak et al., 2014; Carbone and Pierro, 2012; Spuskanyuk et al., 2008). Advances have also been made on understanding the adhesion of fibrillar structures on soft (Cheung and Sitti, 2009) or rough (Cañas et al., 2012; Vajpayee et al., 2010; Wang et al., 2009; Yu et al., 2012) substrates. However, the adhesion of these microstructures to compliant and rough substrates such as tissue or skin is not yet sufficiently understood (Kwak et al., 2011). Furthermore, the shear resistance of fibrillar PDMS microstructures is usually very low due to the relatively low elastic modulus and the high aspect ratio of the fibrils. A promising strategy to enhance the shear resistance is to tailor the materials properties by reinforcing them to create stiffer, but still elastic composite materials. Nature also uses composite materials to tune material properties (Dunlop and Fratzl, 2010; Gorb and Filippov, 2014; Peisker et al., 2013). Recently, studies on composite materials based on PDMS mixtures with different cross-linking densities were performed, with a particular focus on normal adhesion to rigid substrates (Bae et al., 2013b) and to skin (Bae et al., 2013a). Additionally, microstructures with embedded particles have recently been used to tune frictional properties of PDMS at the microscale (Tian et al., 2015) or the normal adhesion forces (Shaikh et al., 2007).

To design and optimize adhesive microstructures for medical applications, systematic knowledge of contact mechanics and the related mechanical properties are urgently needed. Many studies on normal adhesion to different substrates including tissue exist. However, there are applications like hernia meshes where shear adhesion and friction dominate over capabilities of normal adhesion. Despite considerable progress, many aspects of creating shear resistance between surface structures and wet tissue are at present insufficiently understood.

The present work explores, for the first time, the parameter space with regard to elastic modulus for tuning the shear resistance against wet tissue. Pure PDMS was modified by incorporation of submicron polyethylene (PE) particles and by coating with parylene. PE and parylene were chosen because of their higher elastic modulus compared to PDMS and their biocompatibility. The elastic moduli were determined by tensile tests and compared to theoretical models. Pillar structures topped with mushroom-like tip geometries were fabricated by a two-step molding process and sheared against chicken tissue to provide a proof-of-principle for self-fixating medical devices.

## 2. Analytical models

Composites are combinations of at least two materials with the goal to blend their physical or mechanical properties and thereby create a tailored material with superior characteristics for a certain application. In this section, we describe three concepts for calculating the elastic modulus of biphasic composites consisting of a matrix phase and a reinforcing phase such as fibers, layers, whiskers, particulates, or fabrics. The prediction of the elastic modulus is important to predict the mechanical properties of a composite, especially the stiffness and resulting shear resistance.

To a first approximation, a biphasic material can be mechanically modeled as a two-layer composite structure (Fig. 1). The resulting effective elastic modulus is a function of the volume fractions and the elastic moduli of the components involved (Hill, 1963). The Voigt model (Fig. 1a) determines the maximum elastic modulus, $E_{VOIGT}$, by assuming layers under parallel loading with equal strain:

$$E_{VOIGT} = \upsilon_m \cdot E_m + \upsilon_r \cdot E_r, \quad (1)$$

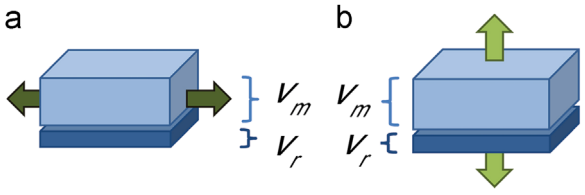


**Fig. 1 – Models for prediction of the elastic modulus of composites. The (a) Voigt and (b) Reuss model are used for modeling biphasic composites.**

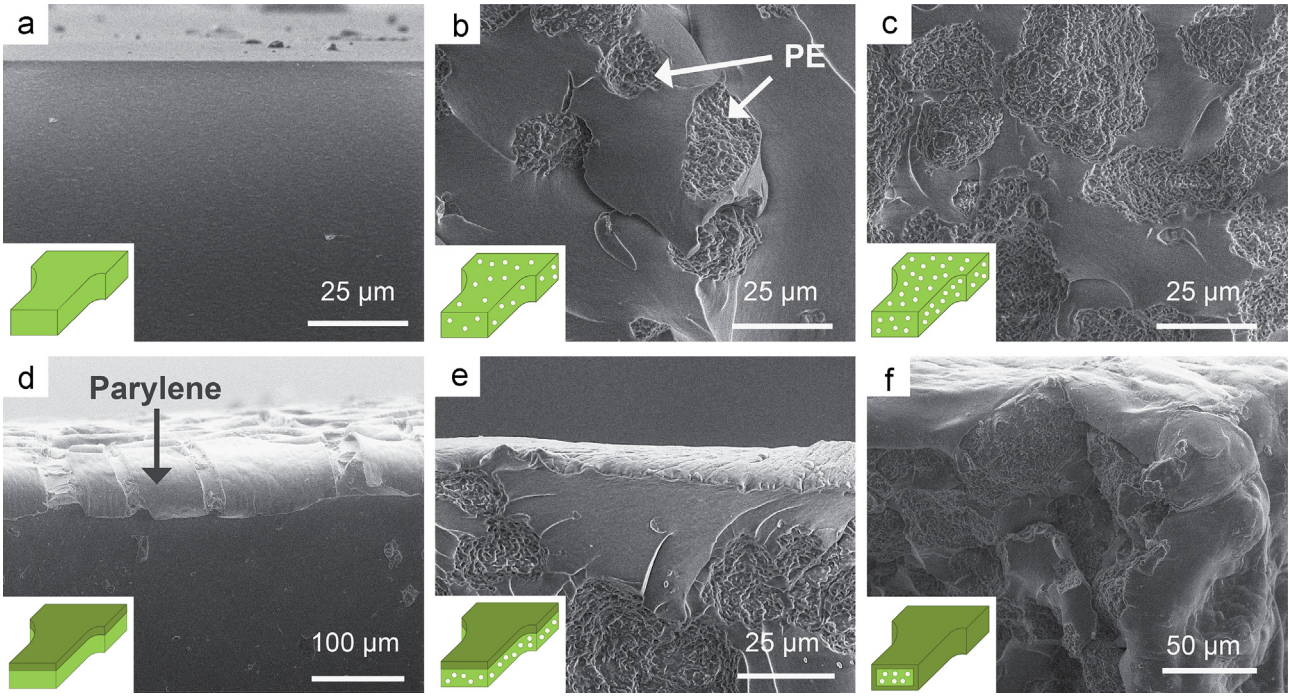


**Fig. 2 – SEM micrographs of the fracture surface after tensile testing and schematic illustrations of the corresponding dogbone samples: (a) pure PDMS material, reinforced with (b) 25 wt% PE particles, (c) 40 wt% PE particles, (d) a one-side parylene coating, (e) a combination of 25 wt% PE particles and one-side parylene coating or (f) 40 wt% PE particles and all outer surfaces parylene coating.**

with $\upsilon_m$ and $\upsilon_r$ the volume fractions and $E_m$ and $E_r$ the elastic moduli of the matrix and the reinforcing material, respectively.

By contrast, the Reuss model (Fig. 1b) determines the minimum elastic modulus, $E_{REUSS}$, by assuming layers under serial loading and equal stress:

$$E_{REUSS}^{-1} = \upsilon_m \cdot E_m^{-1} + \upsilon_r \cdot E_r^{-1}. \quad (2)$$

Numerous models exist to describe the elastic properties for non-laminar composites (Tucker and Liang, 1999). One of them is the Halpin-Tsai model, which accounts for the morphology of the reinforcing phase such as aspect ratio, regularity and shape, as well as the loading direction by an empirical reinforcement factor $\xi$. The model predicts the elastic modulus, $E_{HALPIN-TSAI}$, as follows (Affdl and Kardos, 1976):

$$E_{HALPIN-TSAI} = \frac{E_m \cdot [E_r + \xi \cdot (\upsilon_m \cdot E_m + \upsilon_r \cdot E_r)]}{\upsilon_m \cdot E_r + \upsilon_r \cdot E_m + \xi \cdot E_m}. \quad (3)$$

The reinforcement factor $\xi$ is defined as:

$$\xi = k \cdot \frac{l}{d}, \quad (4)$$

where $\frac{l}{d}$ designates the ratio of the dimension of the reinforcing phase in direction of the loading (l) to the dimension perpendicular to the loading (d). The proportionality factor, $k$, reflects the geometry and the distribution of the reinforcing phase. Hence, the model can, for example, distinguish between long, unidirectional fibers parallel $\left(\frac{l}{d} \to \infty\right)$ or perpendicular $\left(\frac{l}{d} \to 0\right)$ to the loading direction. For spherical particles the ratio $\frac{l}{d}$ is 1. The reinforcement factor $\xi$ can only be determined empirically by fitting experimental data. This was achieved with the materials created for this study as described below.

## 3. Materials and methods

### 3.1. *Composite preparation*

Polydimethylsiloxane (PDMS, Sylgard 184, Dow Corning, Midland, MI, USA) with a mixing ratio of 10 weight parts of the basement to 1 weight part of the curing agent was used as an elastomeric matrix material for all composites.

Polyethylene powder (PE, with particle size from 50 to 70 µm, Sigma-Aldrich, St. Louis, MO, USA) was incorporated into PDMS to manufacture particulate-based composites. After mixing basement and curing agent of PDMS, PE particles of 25 or 40 wt% were immediately added and the mixture was stirred for several minutes. The material was then degassed in an Eppendorf centrifuge 5430 for 2 min at 5000 rpm (Eppendorf, Hauppauge, NY, USA), poured into plastic petri dishes and cured overnight at 70 °C to obtain thin composite films.

Parylene coatings were chosen to fabricate lamellar-based composites. Parylene is a FDA approved, inert, transparent, and hydrophobic thermoplastic biopolymer which forms linear, highly crystalline structures (Shin et al., 2003). Parylene was synthesized by vapor deposition in an SCS Labcoter 2 Parylene Deposition System (SCS, Indianapolis, IN, USA). The final thickness of the parylene coating for all structures was about 5 µm. Parylene fractions from 0.4% to 2% were realized by varying the thickness of the underlying PDMS

films. For tensile tests, two types of dogbone shaped samples were manufactured, with either a one-side coating or a all outer surfaces coating (*cf.* Fig. 2d–f). The final composites were imaged in a scanning electron microscope; see for example Fig. 2 (Quanta 400, FEI, Hillsboro, OR, USA).

### 3.2. *Microstructure fabrication and characterization*

Pillar structures with mushroom-shaped tips were fabricated in a two-step replication process (*cf.* Fig. 6). Two templates were machined from aluminum. Both patterns consisted of cylindrical holes with different diameters and depths, but arranged in hexagonal lattices with a center-to-center spacing of 1.5 mm. The template for the pillar structures had holes with a depth of 1 mm and a diameter of 450 μm. The template for the tip structure consisted of holes with a depth of 200 μm and a diameter of 650 μm. Both templates were coated in a gas phase silanization process using Trichloro (octadecyl)silane (Sigma Aldrich, St. Louis, MO, USA) to obtain a hydrophobic, non-reactive surface. A daughter mold was cast using PDMS. For this, the templates were filled with polymer, degassed for about 20 min under vacuum and cured overnight at 70 °C. For tone inversion, the daughter mold was cast with PDMS again to obtain the final mold used for microstructure fabrication. PDMS molds are much more flexible than the initial aluminum templates and can be reproduced at will. Thus, they are better suited for molding stiffer materials.

To assemble the pillar and tip of the structure, the mold for the pillar structure was first filled with the respective PDMS based composite, degassed and cured overnight at 70 °C. The tip mold was then covered with the respective composite, degassed and the overflow material taken off the surface with a razor blade so that only the cavities remained filled. After that, the fabricated pillar array was manually pushed into the tip mold and cured overnight at 70 °C.

### 3.3. *Tensile tests*

The elastic properties of the samples were measured by tensile tests using dogbone-shaped samples punched from flat films of the respective materials. The gage length varied for each sample and the gage width was 2.79 mm for all samples. The thickness of each sample was measured with a Nikon Eclipse TE2000-U optical microscope (Nikon, Tokyo, Japan) at four different points along the gage length to obtain an average thickness for the stress calculations. All tests were performed, using the table top tester system eXpert 7600 (10 N load cell, ADMET, Norwood, MA, USA), at a constant velocity of 5 mm/min. Force–displacement curves were converted to engineering stress–strain data for analysis using the initial cross-section. The slope of the linear region of the stress–strain curves was used to determine the Young's modulus. Due to viscoelastic contributions, these values will represent lower bounds on the true Young's modulus.

In addition to tensile tests to sample fracture, cyclic tests in the linear elastic region were performed for selected parylene-coated dogbone samples to simulate repetitive loading in a medical application. About 500 cycles were performed with a tensile strain amplitude of 5% at a constant velocity of 5 mm/min. These tests were performed on dry and on moistened samples. For moistening, the samples were wetted with a water droplet which was renewed as soon as the fluid evaporated.

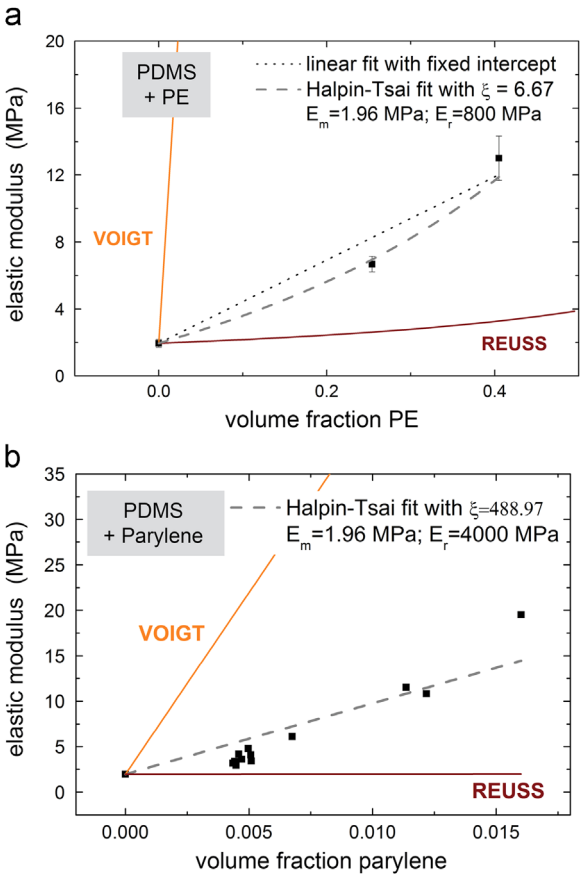


**Fig. 3 – Elastic modulus values determined by tensile tests. Data points (black squares) for (a) PE particulate reinforced PDMS and (b) one-side parylene reinforced PDMS were modeled using the Halpin-Tsai relation (dashed line, *cf.* Eq. (3)). For comparison the upper and lower limit for the material combinations were calculated, i.e. the Voigt (*cf.* Eq. (1)) and Reuss (*cf.* Eq. (2)) model, respectively.**

### 3.4. *Shear tests*

Shear experiments were performed using the biaxial axial-torsion tester eXpert 8600 (10 N load cell, ADMET, Norwood, MA, USA). Chicken thigh was chosen as counter-surface for the experiments since it is a muscular tissue with a relatively homogeneous texture. Fresh chicken thigh was purchased in the supermarket and used for experiments on the same day. The thigh was sliced into about 1 mm thick slices. A tissue slice and a patterned sample were each attached to a glass slide with Loctite superglue (Westlake, OH, USA) in parallel alignment. Three shear cycles with a displacement of 10 mm were performed for each sample. To adjust similar preloads, the samples were placed with the same distance to the tissue before each measurement.

## 4. Results and discussion

SEM micrographs of the fracture surfaces after tensile testing are displayed in Fig. 2. Pure PDMS exhibited a featureless fracture surface (Fig. 2a), whereas PDMS-based composites resulted in dimpled fracture areas attributed to the dispersed PE particles (Figs. 2b and c). The fracture surface of the coated PDMS was again mostly featureless (Fig. 2d), in contrast to the coated PE-PDMS composite samples (Figs. 2e and f). These findings suggest that the PE composites were successfully manufactured. The thickness of the parylene film was determined to be about 5 μm.

The tensile tests revealed an increase of the elastic modulus by a factor of more than 3 for 25 wt% PE-reinforced PDMS and by more than a factor of 6 for 40 wt% PE in comparison to pure PDMS (Fig. 3a). For parylene-coated PDMS, the elastic modulus also increased with increasing parylene content (Fig. 3b). A tenfold increase to 20 MPa compared to the pure base material was measured for 1.6 vol% parylene reinforcement.

These experimental data are in excellent agreement with the Halpin-Tsai equation (Eq. 3) as displayed in Fig. 3. This agreement was obtained with a small geometry factor, $\xi = 6.7$. The particles used for these experiments have a size distribution between 50 and 70 μm, as determined by mesh screening by the manufacturer. Therefore, an aspect ratio close to 1 and a small geometry factor $\xi$ are considered appropriate. The figures also include the wide bounds given by the Voigt and Reuss limits (Eqs. (1) and (2)). The model for parylene-coated PDMS appears linear in this figure, but this is only true for small volume fractions.

For parylene coated PDMS (Fig. 3b), a Halpin-Tsai fit with geometry factor of about $\xi = 489$ was determined to match the experimental data best. Even though parylene was applied as a coating, the Voigt model alone is not sufficient to describe the composite. The factor $\xi$ for the Halpin-Tsai fit of parylene coated PDMS is much higher than the factor for the PE reinforced composite. Higher values of $\xi$ indicate that the aspect ratio of the reinforcing phase increases in loading direction. This is in good agreement with the geometry of the parylene reinforcement, for which a higher $\xi$ value would be expected.

The results of the tensile tests for PDMS and PE reinforced PDMS composites with parylene coatings are summarized in Fig. 4. Due to gripping effects or initial slack in the specimen, the very first portion of the curve will not be considered; the zero point of strain was chosen as indicated in the figure. The curves in Fig. 4a indicate a change in slope between 2.5% and 7% strain at the transition of “Zone 1” to “Zone 2”. The stress at the threshold between both zones correlates roughly with the parylene content. The parylene fraction is determined by the thickness of the base polymer film which was coated, as

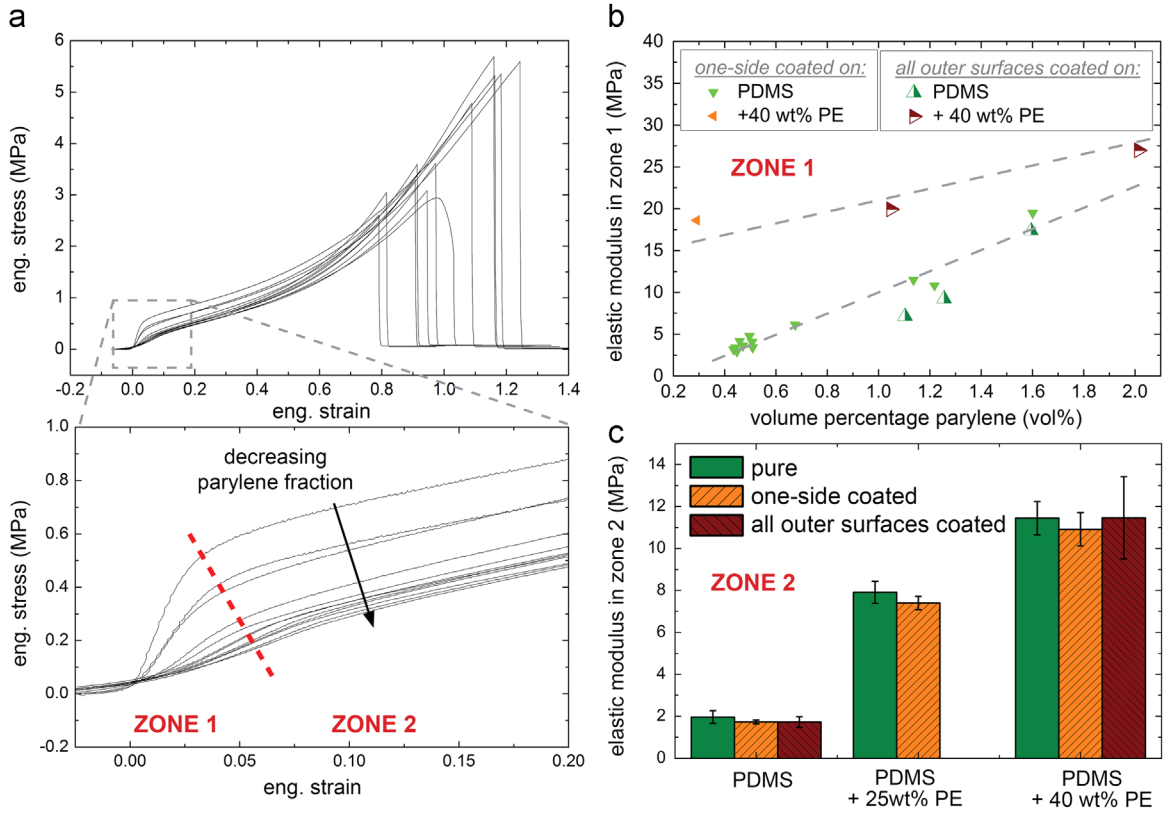


**Fig. 4 – Tensile tests of parylene coated samples. (a) The stress–strain curves of parylene coated PDMS show a change in slope occurring at strains depending on the parylene content. (b) The measured elastic moduli in the first linear region of all parylene reinforced composites depend on the parylene fraction. (c) The slope of the stress–strain curve of the parylene coated materials is in good agreement with uncoated specimens for strains between 10% and 20% strain. The dashed lines in this figure are intended to guide the eye.**

the coating thickness, 5 μm, is constant for all samples. In the first zone, the slope of the curves changes depending on the parylene fraction while the slope is similar regardless of the parylene fraction in Zone 2. This behavior was observed for all parylene coated samples, notably also for 25 and 40 wt% PE reinforced PDMS.

The elastic moduli of pure and 40 wt% PE reinforced PDMS in zone 1 are plotted in Fig. 4b as a function of the volume fraction of parylene. The measured values for all outer surfaces coated dogbones are lower compared to the films with the same matrix, but the elastic modulus increases with increasing parylene content in both cases. This can be attributed overestimation of the parylene content in the all outer surfaces coated samples due to the dogbone shape. From these results we can conclude that the elastic modulus of the materials increased with higher content of parylene for both one-side and all outer surfaces coating.

To investigate whether the transition from Zone 1 to Zone 2 is associated with failure of the parylene layer and Zone 1 represents the elastic deformation of the coating, the slope of the stress–strain curves between 10% and 20% strain was evaluated for all parylene coated materials and uncoated samples as a reference (Fig. 4c). In Zone 2 the elastic modulus of every parylene coated composite corresponds to the one of base material and the reinforcing property of the parylene layer disappears.

The data in Fig. 4a can be explained as follows: during initial load application, the slope of the curves corresponds at first to the elastic modulus of the composite. At the transition stress between Zone 1 and Zone 2, the parylene coating cracks, as can be seen in Fig. 2d. From then on, the slope corresponds to the elastic modulus of the uncoated base material.

The stress strain-behavior in 500 cycles of loading and unloading within Zone 1 only slightly changes between dry and wet conditions (Fig. 5). The composites were not cracked as the maximum strain was chosen below the critical strain for cracking and, thus, can withstand repetitive loading below the critical limit.

To test if the promising properties of the composites can be used for microstructures, pillar structures with mushroom-shaped tips were fabricated in a two-step replication process (Fig. 6) as previously described in Section 3. Fig. 6 also shows exemplary pictures of the manufactured structures from pure PDMS. All other composites were also successfully used to make microstructures. Five composites were selected to be compared regarding their shear resistance against chicken tissue in shear experiments.

Fig. 7a illustrates the characteristic shape of a measured shear hysteresis. The sample (shown in blue), was brought in contact with the tissue (pink) (1) and a lateral shear movement was applied. The pillars were bent against the direction of motion (2) until a constant force plateau was reached representing interlocking with the tissue and sliding friction. Thereafter, the direction of displacement was reversed. In the first part of the reverse half-cycle, the pillars were bent in motion direction (3) until this configuration became unstable and an inversion of pillar orientation took place (4). A constant force plateau was again recorded due to interlocking with the tissue (5). The shape of the two following cycles was found to be similar. The first half-cycle differed from the following ones because of a different initial orientation of the pillars. The shear resistance was defined as the maximum shear force corresponding to the average of the absolute values of both plateaus indicated in Fig. 7a due to the symmetry of the characteristic shear hysteresis. The obtained force–displacement curve as well as the shear resistance may vary with the preload and the experimental setup, which were both kept constant in our experiments.

Fig. 7b displays the shear resistance against chicken tissue of the four composite microstructures in comparison to the pure PDMS. All composite microstructures showed increased shear resistance compared to pure PDMS. Overall, the shear resistance increases nearly linearly with increasing elastic modulus (Fig. 7c). Beam theory predicts the bending stiffness of a beam to be proportional to the elastic modulus, $E$. This is in good agreement with the experimental data described herein. Additionally, the forces measured over the three shear cycles do not show large deviations. This was observed for all samples, especially also for the parylene-coated ones.

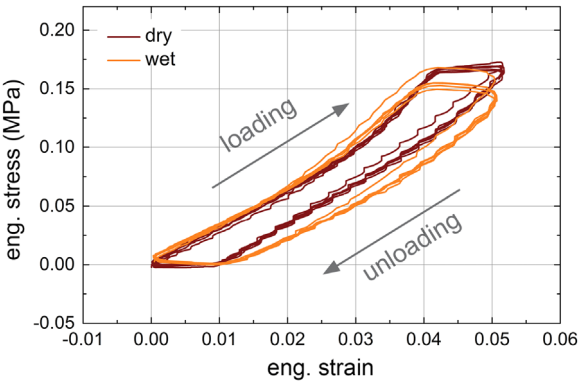


**Fig. 5 – Cyclic tensile tests under dry and wet conditions. 500 cycles were performed on one-side coated PDMS samples with a maximum of 0.5% tensile strain aiming to stay within zone 1 (*cf.* Fig. 4a). The graph shows the first cycle and every 100th cycle thereafter.**

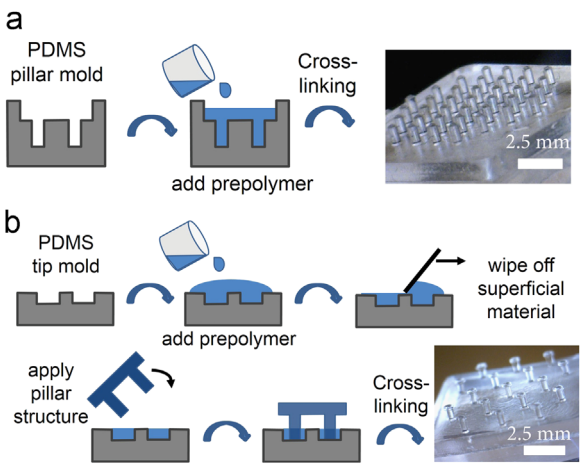


**Fig. 6 – Microstructure fabrication process. Schematic for simple pillar structures (a) and for pillar structures with mushroom tips (b). Exemplary optical pictures are shown on the right.**

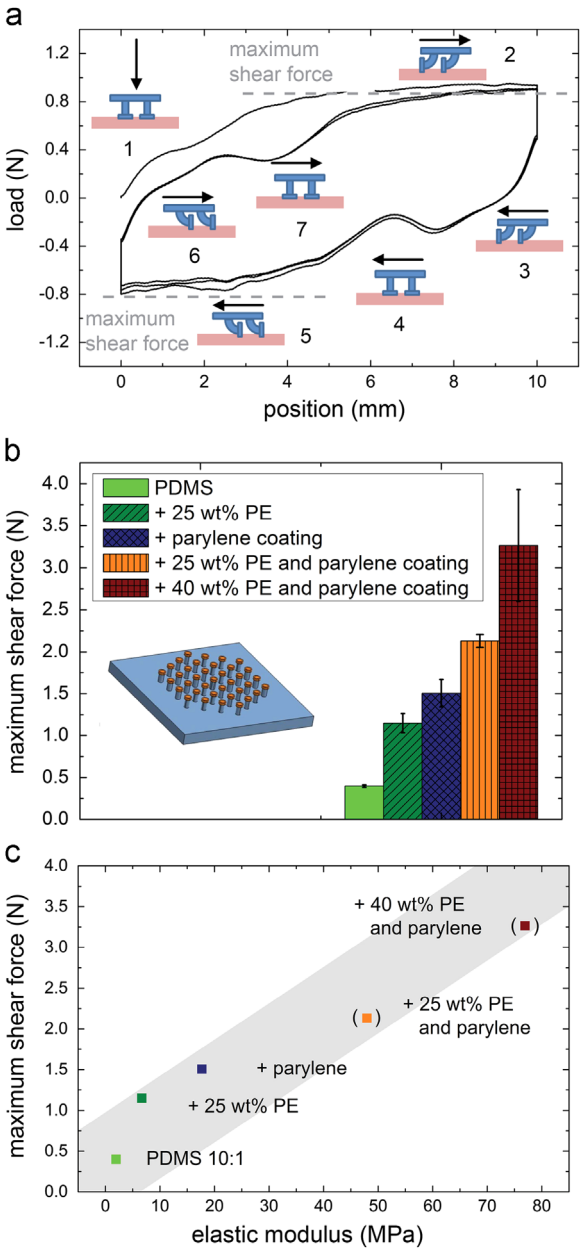


**Fig. 7 – Shear experiments of micropatterned composite surfaces against tissue. (a) Characteristic shear hysteresis, (b) maximum shear force of microstructures manufactured from pure PDMS and PDMS composites and (c) correlation of those shear force values with the elastic modulus of the composites. The values in brackets are estimates and were calculated using Eq. (3) with the elastic modulus of the PE composite as $E_m$, $E_r = 4000$ MPa and the reinforcement factor $\xi = 488.9$. The volume fraction parylene in the pillar region of the microstructure was estimated to be $v_r = 0.02$ and used for the calculations. The grey region shows the approximately linear relationship between shear force and elastic modulus.**

This indicated that the patterned surfaces stayed intact, which could also be observed upon testing.

Overall, our experiments underline the feasibility of incorporating PDMS based composites in a molding process to fabricate robust interlocking microstructures. The results suggest that the shear resistance, which will control the interlocking action in closing a wound or in fixating an implant or mesh, is correlated with the modulus of the material used for the microstructures. Our results suggest that the composite approach can enable tunable microstructures for medical applications covering a wide range of wound and tissue characteristics.

## 5. Conclusions

In this study, the potential of PDMS based composites for interlocking microstructures in medical applications was investigated. PDMS based composites were manufactured with PE particulate, a parylene coating reinforcement and a combination of both. Different PDMS composites were integrated in a multiple-molding process and mushroom-like interlocking structures were successfully manufactured. The shear resistance was then measured cyclically against chicken thigh muscle. The following conclusions can be drawn:

1. The composite approach allowed the modulus of PDMS to be increased by over an order of magnitude (from 2 to 27 MPa), in good agreement with the Halpin-Tsai equation.
2. At the same time, the high fidelity molding properties of PDMS were preserved. Patterned microstructures could be fabricated from multiple composite materials.
3. Shear testing against chicken muscle resulted in characteristic force–displacement hysteresis curves. We demonstrated the long-term stability of the response under dry and wet conditions in cyclic experiments of more than 500 cycles. The hysteresis was affected by incorporation of PE particles or coating with parylene. The shear resistance was found to correlate with the modulus of the material, in good agreement with beam theory. Additionally the point of pillar orientation inversion can be tuned.
4. The proposed approach is a proof-of-principle for customizing the shear characteristics of microstructures by tuning their elastic modulus. Before such structures can become useful for medical applications such as wound closure, further *in vivo* and long-term experiments are warranted.

## Acknowledgments

The authors would like to acknowledge Dr. Nathalie Guimard for valuable discussions and Dr. Girish Chitnis for his help with the parylene coating. Uwe Magar and Herbert Beermann, from the INM engineering team, kindly manufactured the microstructure templates. Partial funding from the European Research Council under the European Union's Seventh Framework Programme (FP/2007-2013)/ERC Grant Agreement no. 340929 (to EA) and from the NIH grant GM086433 (to JMK) is acknowledged.

## REFERENCES


Affdl, J.C., Kardos, J.L., 1976. The Halpin-Tsai equations: a review. Polym. Eng. Sci. 16, 344–352.

Aksak, B., Sahin, K., Sitti, M., 2014. The optimal shape of elastomer mushroom-like fibers for high and robust adhesion. Beilstein J. Nanotechnol. 5, 630–638, http://dx.doi.org/10.3762/bjnano.5.74.

Arzt, E., Gorb, S., Spolenak, R., 2003. From micro to nano contacts in biological attachment devices. Proc. Natl. Acad. Sci. USA 100, 10603–10606, http://dx.doi.org/10.1073/pnas.1534701100.

Bae, W.G., Kim, D., Kwak, M.K., Ha, L., Kang, S.M., Suh, K.Y., 2013a. Enhanced skin adhesive patch with modulus-tunable composite micropillars. Adv. Healthc. Mater. 2, 109–113, http://dx.doi.org/10.1002/adhm.201200098.

Bae, W.G., Kwak, M.K., Jeong, H.H.E., Pang, C., Jeong, H.H.E., Suh, K.-Y., 2013b. Fabrication and analysis of enforced dry adhesives with core–shell micropillars. Soft Matter 9, 1422, http://dx.doi.org/10.1039/c2sm27323c.

Bennett, R.G., 1988. Selection of wound closure materials. J. Am. Acad. Dermatol. 18, 619–637, http://dx.doi.org/10.1016/S0190-9622(88)70083-3.

Bin Khaled, W., Sameoto, D., 2014. Fabrication and characterization of thermoplastic elastomer dry adhesives with high strength and low contamination. ACS Appl. Mater. Interfaces 6, 6806–6815, http://dx.doi.org/10.1021/am500616a.

Birk, D., Pardo, C.G., 2012. Self-gripping Parietene and Parietex Progrip mesh laparoscopic hernia repair: have we found the ideal implant?. Surg. Technol. Int. 22, 93–100.

Brown, C.N., Finch, J.G., 2010. Which mesh for hernia repair?. Ann. R. Coll. Surg. Engl. 92, 272.

Cañas, N., Kamperman, M., Völker, B., Kroner, E., McMeeking, R. M., Arzt, E., 2012. Effect of nano- and micro-roughness on adhesion of bioinspired micropatterned surfaces. Acta Biomater. 8, 282–288, http://dx.doi.org/10.1016/j.actbio.2011.08.028.

Carbone, G., Pierro, E., 2012. Sticky bio-inspired micropillars: finding the best shape. Small 8, 1449–1454, http://dx.doi.org/10.1002/smll.201102021.

Chary, S., Tamelier, J., Turner, K., 2013. A microfabricated gecko-inspired controllable and reusable dry adhesive. Smart Mater. Struct. 22, 025013, http://dx.doi.org/10.1088/0964-1726/22/2/025013.

Chastan, P., 2009. Tension-free open hernia repair using an innovative self-gripping semi-resorbable mesh. Hernia 13, 137–142, http://dx.doi.org/10.1007/s10029-008-0451-4.

Cheung, E., Sitti, M., 2009. Adhesion of biologically inspired polymer microfibers on soft surfaces. Langmuir 25, 6613–6616, http://dx.doi.org/10.1021/la900997p.

Cho, W.K., Ankrum, J.A., Guo, D., Chester, S.A., Yang, S.Y., Kashyap, A., Campbell, G.A., Wood, R.J., Rijal, R.K., Karnik, R., Langer, R., Karp, J.M., 2012. Microstructured barbs on the North American porcupine quill enable easy tissue penetration and difficult removal. Proc. Natl. Acad. Sci. USA 109, 21289–21294, http://dx.doi.org/10.1073/pnas.1216441109.

Chu, C.-C., von Fraunhofer, J.A., Greisler, H.P., 1996. Wound Closure Biomaterials and Devices. CRC Press, USA.

Cobb, W.S., Burns, J.M., Peindl, R.D., Carbonell, A.M., Matthews, B. D., Kercher, K.W., Heniford, B.T., 2006. Textile analysis of heavy weight, mid-weight, and light weight polypropylene mesh in a porcine ventral hernia model. J. Surg. Res. 136, 1–7.

Del Campo, A., Greiner, C., Arzt, E., 2007. Contact shape controls adhesion of bioinspired fibrillar surfaces. Langmuir 23, 10235–10243, http://dx.doi.org/10.1021/la7010502.

Dunlop, J.W.C., Fratzl, P., 2010. Biological Composites. Annu. Rev. Mater. Res. 40, 1–24, http://dx.doi.org/10.1146/annurev-matsci-070909-104421.

Glass, P., Chung, H., Washburn, N.R., Sitti, M., 2010. Enhanced wet adhesion and shear of elastomeric micro-fiber arrays with mushroom tip geometry and a photopolymerized p(DMA-co-MEA) tip coating. Langmuir 26, 17357–17362, http://dx.doi.org/10.1021/la1029245.

Gorb, S., Gorb, E., Kastner, V., 2001. Scale effects on the attachment pads and friction forces in syrphid flies (Diptera, Syrphidae). J. Exp. Biol. 204, 1421–1431.

Gorb, S.N., 1998. Frictional surfaces of the elytra-to-body arresting mechanism in tenebrionid beetles (Coleoptera: Tenebrionidae): design of co-opted fields of microtrichia and cuticle ultrastructure. Int. J. Insect Morphol. Embryol. 27, 205–225, http://dx.doi.org/10.1016/S0020-7322(98)00013-0.

Gorb, S.N., Filippov, A.E., 2014. Fibrillar adhesion with no clusterisation: functional significance of material gradient along adhesive setae of insects. Beilstein J. Nanotechnol. 5, 837–845, http://dx.doi.org/10.3762/bjnano.5.95.

Gorb, S.N., Sinha, M., Peressadko, A., Daltorio, K.A., Quinn, R.D., 2007. Insects did it first: a micropatterned adhesive tape for robotic applications. Bioinspired Biomim. 2, S117–S125, http://dx.doi.org/10.1088/1748-3182/2/4/S01.

Hill, R., 1963. Elastic properties of reinforced solids: some theoretical principles. J. Mech. Phys. Solids 11, 357–372, http://dx.doi.org/10.1016/0022-5096(63)90036-X.

Hollinsky, C., Kolbe, T., Walter, I., Joachim, A., Sandberg, S., Koch, T., Rülicke, T., 2009. Comparison of a new self-gripping mesh with other fixation methods for laparoscopic hernia repair in a rat model. J. Am. Coll. Surg. 208, 1107–1114, http://dx.doi.org/10.1016/j.jamcollsurg.2009.01.046.

Jorgensen, L.N., Sommer, T., Assaadzadeh, S., Strand, L., Dorfelt, A., Hensler, M., Rosenberg, J., Danish Multicentre DANGRIP Study Group, 2013. Randomized clinical trial of self-gripping mesh versus sutured mesh for Lichtenstein hernia repair. Br. J. Surg. 100, 474–481, http://dx.doi.org/10.1002/bjs.9006.

Koch, K., Bhushan, B., Barthlott, W., 2009. Multifunctional surface structures of plants: an inspiration for biomimetics. Prog. Mater. Sci.http://dxdoi.org/10.1016/j.pmatsci.2008.07.003.

Kolbe, T., Hollinsky, C., Walter, I., Joachim, A., Rülicke, T., 2010. Influence of a new self-gripping hernia mesh on male fertility in a rat model. Surg. Endosc. 24, 455–461.

Kwak, M.K., Jeong, H.-E., Suh, K.Y., 2011. Rational design and enhanced biocompatibility of a dry adhesive medical skin patch. Adv. Mater. 23, 3949–3953, http://dx.doi.org/10.1002/adma.201101694.

Lee, C., Kim, S.M., Kim, Y.J., Choi, Y.W., Suh, K., Pang, C., Choi, M., 2015. Robust microzip fastener: repeatable interlocking using polymeric rectangular parallelepiped arrays. ACS Appl. Mater. Interfaceshttp://dxdoi.org/10.1021/am507559d.

Menaker, G.M., 2001. Wound closure materials in the new millennium. Curr. Probl. Dermatol. 13, 90–94, http://dx.doi.org/10.1016/S1040-0486(01)70039-7.

Pang, C., Kim, T.il, Bae, W.G., Kang, D., Kim, S.M., Suh, K.Y., 2012. Bioinspired reversible interlocker using regularly arrayed high aspect-ratio polymer fibers. Adv. Mater. 24, 475–479, http://dx.doi.org/10.1002/adma.201103022.

Pang, C., Koo, J.H., Nguyen, A., Caves, J.M., Kim, M.-G., Chortos, A., Kim, K., Wang, P.J., Tok, J.B.-H., Bao, Z., 2015. Highly skin-conformal microhairy sensor for pulse signal amplification. Adv. Mater. 27, 634–640, http://dx.doi.org/10.1002/adma.201403807.

Pang, C., Lee, C., Suh, K.-Y., 2013. Recent advances in flexible sensors for wearable and implantable devices. J. Appl. Polym. Sci. 130, 1429–1441, http://dx.doi.org/10.1002/app.39461.

Paretkar, D., Kamperman, M., Martina, D., Zhao, J., Creton, C., Lindner, A., Jagota, A., McMeeking, R., Arzt, E., 2013. Preload-responsive adhesion: effects of aspect ratio, tip shape and alignment. J. R. Soc. Interface 10, 20130171, http://dx.doi.org/10.1098/rsif.2013.0171.

Pedano, N., Pastor, C., Arredondo, J., Poveda, I., Ruiz, J., Montón, S., Molina, M., Hernández-Lizoain, J.L., 2012. Open tension-free hernioplasty using a novel lightweight self-gripping mesh: medium-term experience from two institutions. Langenbeck's Arch. Surg. 397, 291–295.

Peisker, H., Michels, J., Gorb, S.N., 2013. Evidence for a material gradient in the adhesive tarsal setae of the ladybird beetle Coccinella septempunctata. Nat. Commun. 4, 1661, http://dx.doi.org/10.1038/ncomms2576.

Ratner, B.D., Bryant, S.J., 2004. BIOMATERIALS: where we have been and where we are going. Annu. Rev. Biomed. Eng. 6, 41–75, http://dx.doi.org/10.1146/annurev.bioeng.6.040803.140027.

Sanders, D., Lambie, J., Bond, P., Moate, R., Steer, J.A., 2013. An in vitro study assessing the effect of mesh morphology and suture fixation on bacterial adherence. Hernia 17, 779–789, http://dx.doi.org/10.1007/s10029-013-1124-5.

Scheidel, P., Hohl, M.K., 1987. 1 Modern synthetic suture materials and abdominal wound closure techniques in gynaecological surgery. Bailliere's Clin. Obstet. Gynaecol. 1, 223–246, http://dx.doi.org/10.1016/S0950-3552(87)80052-4.

Shaikh, S., Birdi, A., Qutubuddin, S., Lakatosh, E., Baskaran, H., 2007. Controlled release in transdermal pressure sensitive adhesives using organosilicate nanocomposites. Ann. Biomed. Eng. 35, 2130–2137, http://dx.doi.org/10.1007/s10439-007-9369-8.

Shin, Y.S., Cho, K., Lim, S.H., Chung, S., Park, S.-J., Chung, C., Han, D.-C., Chang, J.K., 2003. PDMS-based micro PCR chip with Parylene coating. J. Micromech. Microeng. 13, 768–774, http://dx.doi.org/10.1088/0960-1317/13/5/332.

Spuskanyuk, A.V., McMeeking, R.M., Deshpande, V.S., Arzt, E., 2008. The effect of shape on the adhesion of fibrillar surfaces. Acta Biomater. 4, 1669–1676, http://dx.doi.org/10.1016/j.actbio.2008.05.026.

Tian, Y., Zhao, Z., Zaghi, G., Kim, Y., Zhang, D., Maboudian, R., 2015. Tuning the friction characteristics of gecko-inspired polydimethylsiloxane micropillar arrays by embedding $Fe_3O_4$ and $SiO_2$ particles. ACS Appl. Mater. Interfaces 7, 13232–13237, http://dx.doi.org/10.1021/acsami.5b03301.

Tucker, C.L., Liang, E., 1999. Stiffness predictions for unidirectional short-fiber composites: review and evaluation. Compos. Sci. Technol. 59, 655–671.

Vajpayee, S., Jagota, A., Hui, C.-Y., 2010. Adhesion of a fibrillar interface on wet and rough surfaces. J. Adhes.http://dxdoi.org/10.1080/00218460903417834.

Wang, J., Qian, J., Gao, H., 2009. Effects of capillary condensation in adhesion between rough surfaces. Langmuir 25, 11727–11731, http://dx.doi.org/10.1021/la900455k.

Yang, S.Y., O'Cearbhaill, E.D., Sisk, G.C., Park, K.M., Cho, W.K., Villiger, M., Bouma, B.E., Pomahac, B., Karp, J.M., 2013. A bio-inspired swellable microneedle adhesive for mechanical interlocking with tissue. Nat. Commun. 4, 1702.

Yu, J., Chary, S., Das, S., Tamelier, J., Turner, K.L., Israelachvili, J.N., 2012. Friction and adhesion of Gecko-Inspired PDMS flaps on rough surfaces. Langmuir 28, 11527–11534, http://dx.doi.org/10.1021/la301783q.

Zhang, C., Li, F., Zhang, H., Zhong, W., Shi, D., Zhao, Y., 2013. Self-gripping versus sutured mesh for inguinal hernia repair: a systematic review and meta-analysis of current literature. J. Surg. Res. 185, 653–660, http://dx.doi.org/10.1016/j.jss.2013.07.035.

Zhou, M., Pesika, N., Zeng, H., Tian, Y., Israelachvili, J., 2013. Recent advances in gecko adhesion and friction mechanisms and development of gecko-inspired dry adhesive surfaces. Friction 1, 114–129, http://dx.doi.org/10.1007/s40544-013-0011-5.